Pten controls lung morphogenesis, bronchioalveolar stem cells, and onset of lung adenocarcinomas in mice

Shigehisa Yanagi,[1,2] Hiroyuki Kishimoto,[1] Kohichi Kawahara,[1,3] Takehiko Sasaki,[4] Masato Sasaki,[1] Miki Nishio,[1] Nobuyuki Yajima,[1] Koichi Hamada,[1] Yasuo Horie,[5] Hiroshi Kubo,[6] Jeffrey A. Whitsett,[7] Tak Wah Mak,[8] Toru Nakano,[9] Masamitsu Nakazato,[2] and Akira Suzuki[1,3]

[1]Department of Molecular Biology, Akita University School of Medicine, Akita, Japan. [2]Division of Neurology, Respirology, Endocrinology and Metabolism, Third Department of Internal Medicine, Miyazaki Medical College, University of Miyazaki, Miyazaki, Japan. [3]Division of Embryonic and Genetic Engineering, Medical Institute of Bioregulation, Kyushu University, Fukuoka, Japan. [4]Department of Microbiology and [5]Department of Gastroenterology, Akita University School of Medicine, Akita, Japan. [6]Department of Geriatric and Respiratory Medicine, Tohoku University School of Medicine, Sendai, Japan. [7]Division of Pulmonary Biology, Cincinnati Children's Hospital Medical Center, Cincinnati, Ohio, USA. [8]The Campbell Family Institute for Breast Cancer Research and Departments of Immunology and Medical Biophysics, University of Toronto, Toronto, Ontario, Canada. [9]Department of Pathology, Medical School, and Graduate School of Frontier Biosciences, Osaka University, Suita, Osaka, Japan.

***PTEN* is a tumor suppressor gene mutated in many human cancers. We generated a bronchioalveolar epithelium–specific null mutation of *Pten* in mice [*SP-C-rtTA/(tetO)$_7$-Cre/Pten$^{flox/flox}$* (*SOPten$^{flox/flox}$*) mice] that was under the control of doxycycline. Ninety percent of *SOPten$^{flox/flox}$* mice that received doxycycline in utero [*SOPten$^{flox/flox}$*(E10–16) mice] died of hypoxia soon after birth. Surviving *SOPten$^{flox/flox}$*(E10–16) mice and mice that received doxycycline postnatally [*SOPten$^{flox/flox}$*(P21–27) mice] developed spontaneous lung adenocarcinomas. Urethane treatment accelerated number and size of lung tumors developing in *SOPten$^{flox/flox}$* mice of both ages. Histological and biochemical examinations of the lungs of *SOPten$^{flox/flox}$*(E10–16) mice revealed hyperplasia of bronchioalveolar epithelial cells and myofibroblast precursors, enlarged alveolar epithelial cells, and impaired production of surfactant proteins. Numbers of bronchioalveolar stem cells (BASCs), putative initiators of lung adenocarcinomas, were increased. Lungs of *SOPten$^{flox/flox}$*(E10–16) mice showed increased expression of Spry2, which inhibits the maturation of alveolar epithelial cells. Levels of Akt, c-Myc, Bcl-2, and Shh were also elevated in *SOPten$^{flox/flox}$*(E10–16) and *SOPten$^{flox/flox}$*(P21–27) lungs. Furthermore, *K-ras* was frequently mutated in adenocarcinomas observed in *SOPten$^{flox/flox}$*(P21–27) lungs. These results indicate that Pten is essential for both normal lung morphogenesis and the prevention of lung carcinogenesis, possibly because this tumor suppressor is required for BASC homeostasis.**

Introduction

Lung cancer is the leading cause of death due to cancer all over the world, and the 5-year survival rate remains relatively poor despite aggressive medical therapy (1). Adenocarcinoma is the most common type of lung cancer in the United States, and its frequency is increasing rapidly (2, 3). As with most cancers, lung cancer appears to arise by a transformation of organ-specific stem cells or progenitor cells that results in the selective expression of genes enhancing self-renewal potential (2, 4). In this light, stem cells can be considered proto-tumorigenic, in that they must first undergo genetic mutation before they can initiate cancers (2).

Three types of organ-specific stem cells are thought to play key roles in maintaining the epithelial layers of lung tissue. The first type is the basal cell, which generates Clara cells and ciliated cells and is located at the submucosal gland duct junctions or intracartilaginous boundaries of the proximal airway. The second stem cell type is the variant Clara cell, which also generates Clara cells as well as bronchial and bronchiolar neuroendocrine cells and is located adjacent to neuroepithelial bodies in the bronchi/bronchioles. The third stem cell type is the bronchioalveolar stem cell (BASC), which generates Clara cells and alveolar type I (AE-I) and AE-II epithelial cells and is located at the bronchioalveolar duct junction (2). Among these putative stem cell types, it is the BASCs that have recently been proven to exhibit self renewal and multipotency, properties characteristic of stem cells. Importantly, BASCs have been shown to give rise to lung adenocarcinomas (5). Overexpression of K-ras increases the proliferation of BASCs both in vitro and in vivo, whereas this increased proliferation is not seen in cultured differentiated alveolar cells that overexpress K-ras (5). It is not known what molecules in addition to K-ras have positive or negative regulatory effects on BASCs.

Pten is a multifunctional phosphatase whose major substrate is phosphatidylinositol-3,4,5-triphosphate (PIP3) (6), a lipid second messenger molecule. PIP3 is generated by the action of PI3K that has been activated in response to various growth factors (7). PIP3 in turn activates numerous downstream targets, including the serine/threonine kinase Akt/protein kinase B involved in antiapoptosis, proliferation, and oncogenesis (8). By using its lipid phosphatase activity to dephosphorylate PIP3 at the cell membrane, Pten negatively regulates the PI3K/Akt pathway and exerts tumor suppression. In addition, recent studies have shown that

Nonstandard abbreviations used: AE-I, alveolar type I epithelial; AQP5, aquaporin-5; BASC, bronchioalveolar stem cell; CCSP, Clara cell secretory protein; CGRP, calcitonin gene–related peptide; IHC, immunohistochemical; PIP3, phosphatidylinositol-3,4,5-triphosphate; rtTA, reverse tetracycline transactivator; SP, surfactant protein.

Conflict of interest: The authors have declared that no conflict of interest exists.

Citation for this article: *J. Clin. Invest.* **117**:2929–2940 (2007). doi:10.1172/JCI31854.

Table 1
SOPten$^{flox/flox}$ (E10–E16) mice suffer neonatal lethality

	WT(E10–E16)	*SOPten*$^{flox/flox}$(E10–E16)
Alive (n = 28)	25	3
Dead (n = 22)	1	21

Genotyping of P0 mice derived from *(tetO)$_7$-Cre/Pten*$^{flox/flox}$ female and *SP-C-rtTA/(tetO)$_7$-Cre/Pten*$^{flox/flox}$ male intercrosses.

Pten is required for the maintenance of organ-specific stem/progenitor cells in adult brain (9), prostate (10), and blood cells (11), as well as germ cells in the embryo (12).

While mutation of the *PTEN* gene itself is an infrequent event in lung adenocarcinomas (13, 14), loss of PTEN protein expression is seen in 39%–77% of these tumors (14, 15). Indeed, loss of PTEN expression leading to Akt activation correlates positively with a poor prognosis for patients with non–small cell lung cancers, including adenocarcinomas (15). In vitro, lung adenocarcinoma cells treated with siRNA to inactivate Akt fail to proliferate in response to fibronectin (16). These observations support a profound involvement of the PI3K/PTEN/Akt pathway in the development of lung adenocarcinomas.

In addition to its function as a tumor suppressor, Pten plays a critical role in the development of various murine tissues, including T cells (17), B cells (18), endothelial cells (19), and germ cells (12). Whether Pten also influences lung development is currently unknown. The development of lung tissue is an intricate process that involves branching morphogenesis and complex pathways of epithelial and mesenchymal cell differentiation. Based on histology, embryonic lung development can be divided into the pseudoglandular stage (E9.5–E16.5), the canalicular stage (E16.6–E17.4), and the terminal sac stage (E17.5–P0) (20). To date, the only information available on Pten function in the lung is that high levels of Pten expression occur in the respiratory epithelium at the terminal sac stage (21). To thoroughly investigate the roles of Pten in normal lung development and the prevention of tumorigenesis, we generated mice deficient for Pten specifically in bronchioalveolar epithelial cells. Our results provide the first comprehensive evidence that Pten is essential for normal lung morphogenesis, the homeostasis of BASCs, and the prevention of lung adenocarcinomas.

Results

Generation of bronchioalveolar epithelium–specific Pten-deficient mice. Bronchioalveolar epithelium–specific Pten-deficient mice [*SP-C-rtTA/(tetO)$_7$-Cre/Pten*$^{flox/flox}$ mice, referred to here as *SOPten*$^{flox/flox}$ mice] were generated by mating *(tetO)$_7$-Cre* transgenic mice (22) with *SP-C-rtTA* (23) and *Pten*$^{flox/flox}$ mice, in which *Pten* exon 5 encoding the phosphatase domain is flanked by *loxP* sequences (24). Administration of doxycycline either in utero (E10–E16) or postnatally (P21–P27 or P84–P90) activates expression of Cre in combination with reverse tetracycline transactivator (rtTA) (23), which triggers recombination and deletion of the floxed *Pten* gene. Southern blotting of DNA from whole lung tissue of 8-week-old *SOPten*$^{flox/flox}$(E10–E16) mice showed that Cre-mediated recombination of the *loxP* sites had deleted most of the 6.0-kb *Pten*^{flox} allele in a majority of cells, leaving the 2.3-kb *PtenΔ* allele (Supplemental Figure 1A; supplemental material available online with this article; doi:10.1172/JCI31854DS1). Western blotting confirmed a dramatic reduction of Pten protein in lungs of 8-week-old *SOPten*$^{flox/flox}$(E10–E16) mice (Supplemental Figure 1B).

Impaired lung morphogenesis in SOPten$^{flox/flox}$*(E10–E16) mice.* Intercrossing of *(tetO)$_7$-Cre/Pten*$^{flox/flox}$ and *SOPten*$^{flox/flox}$ mice generated *SOPten*$^{flox/flox}$ pups that were born at the expected Mendelian ratio. However, about 90% of *SOPten*$^{flox/flox}$(E10–E16) mice died within 2 hours of birth (Table 1). In contrast to WT(E10–E16) neonates, which breathed regularly, were well oxygenated, and actively moved their limbs, *SOPten*$^{flox/flox}$(E10–E16) neonates breathed irregularly with gasping and had a cyanotic skin color (Figure 1A). Arterial blood gas analyses confirmed the presence of marked hypoxia and respiratory acidosis in *SOPten*$^{flox/flox}$(E10–E16) neonates (Table 2). *SOPten*$^{flox/flox}$(P21–P27) and *SOPten*$^{flox/flox}$(P84–P90) mice did not show any neonatal lethality.

Histologically, lungs of WT(E10–E16) mice showed normal saccular expansion and septal thinning at birth, whereas lungs of *SOPten*$^{flox/flox}$(E10–E16) mice showed notable alveolar septal and bronchiolar hyperplasia with reduced airspaces (Figure 1B). Cell counting confirmed that total cell numbers in *SOPten*$^{flox/flox}$(E10–E16) neonatal lungs were increased 1.5-fold over WT(E10–E16) levels at birth (Figure 1C). Further histological analyses of lungs from WT(E10–E16) and *SOPten*$^{flox/flox}$(E10–E16) embryos at various stages of gestation revealed that loss of Pten delayed lung development at the terminal sac stage (E17.5 to about P0; Figure 1D) but did not affect the pseudoglandular (E14.5; Figure 1D) or canalicular (E16.6; Figure 1D) stages. Specifically, terminal sac–stage (E17.5 to about P0) lungs from WT(E10–E16) animals showed normal progression with the formation of the sac-like structures that serve as precursors of the alveoli (Figure 1D, upper panels). However, terminal sac–stage lungs from *SOPten*$^{flox/flox}$(E10–E16) mice showed a significant delay in the dilatation of the distal tubules (Figure 1D, lower panels).

Ultrastructure analysis by transmission electron microscopy showed marked increases in numbers of both alveolar epithelial cells and mesenchymal cells in lungs of E19.5 *SOPten*$^{flox/flox}$(E10–E16) embryos (Figure 2A). In WT(E10–E16) lungs the septa contained 2 layers of capillaries juxtaposed to the alveolar lumen (Figure 2A, upper left panel). The flat AE-I cells and capillary endothelial cells constituting the blood-air barrier that facilitates efficient gas exchange were clearly visible (Figure 2A, arrowheads). In contrast, the septa of *SOPten*$^{flox/flox}$(E10–E16) lungs contained an increased number of cuboidal undifferentiated alveolar epithelial cells and mesenchymal cells. The size of each alveolar epithelial cell was also increased. Consequently, the blood-air barrier was much thicker in *SOPten*$^{flox/flox}$(E10–E16) lung tissue (Figure 2A, right panels) than in WT(E10–E16) lungs. The increased numbers of alveolar epithelial cells and mesenchymal cells in the mutant lung were caused by enhanced cell proliferation rather than reduced apoptosis at E19.5, as determined by BrdU incorporation (Supplemental Figure 2A) and TUNEL assays (Supplemental Figure 2B). To determine the origin of the expanded mesenchymal cell population, immunohistochemical (IHC) analysis was performed using anti-CD31, anti–α-SMA, anti-desmin, and anti–glial fibrillary acidic protein (anti-GFAP) antibodies. As shown in Supplemental Figure 3, the septa of *SOPten*$^{flox/flox}$(E10–E16) lungs exhibited a marked increase in cells that were α-SMA positive but desmin negative. Cells with this surface marker expression pattern are reportedly precursors of myofibroblasts (25).

Taken together, these results indicate that the abnormal thickness of the blood-air barrier in *SOPten*$^{flox/flox}$(E10–E16) lungs is the

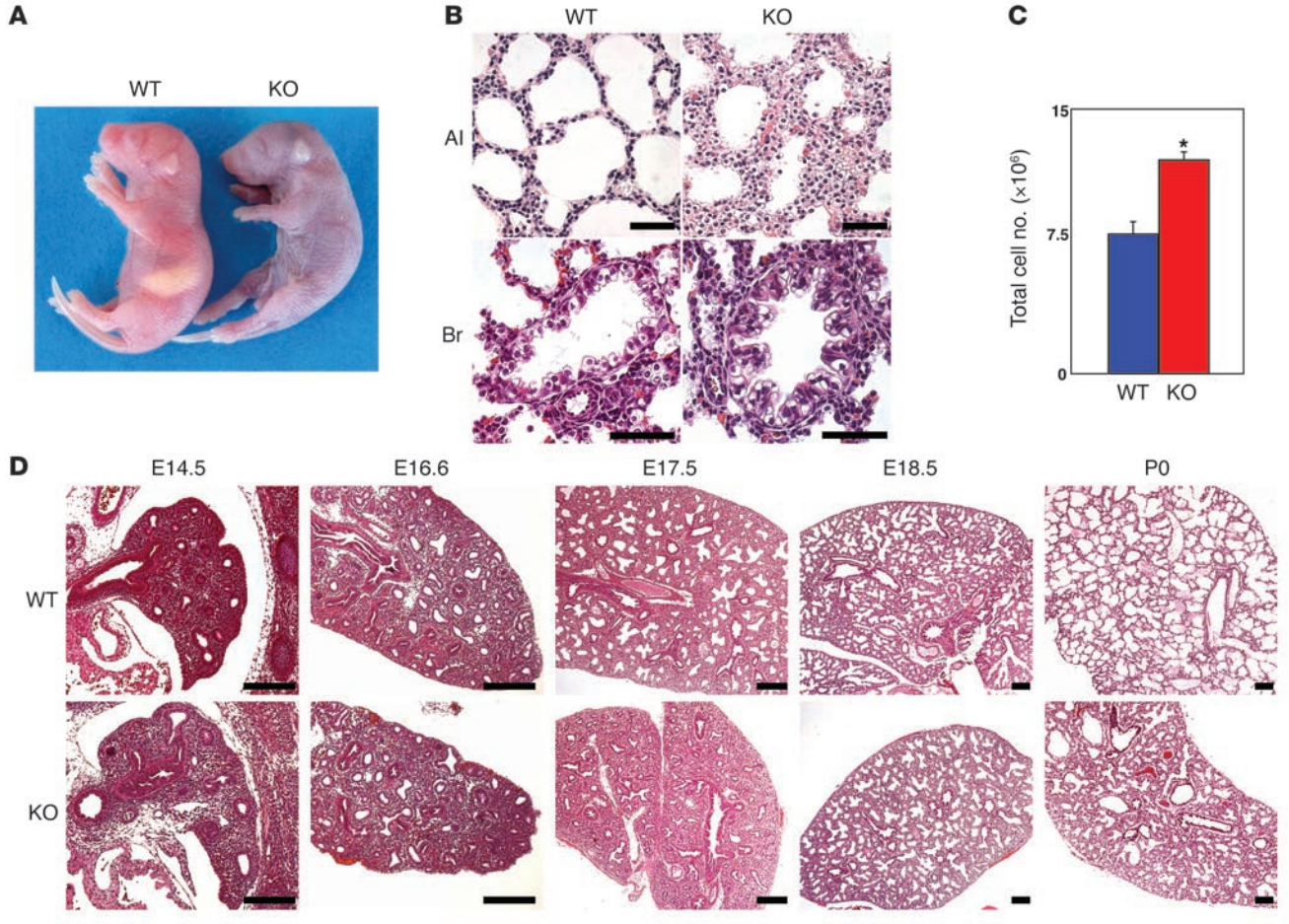

Figure 1
Abnormal lung morphogenesis and lung epithelial cell hyperplasia in *SOPten*$^{flox/flox}$(E10–E16) mice. (**A**) Gross appearance of representative neonates. Skin color is normal in WT(E10–E16) neonates but cyanotic in *SOPten*$^{flox/flox}$(E10–E16) (KO) littermates. (**B**) Histologic analysis of neonatal lungs. Left: normal alveolar (Al) and bronchiolar (Br) epithelial cells from a WT(E10–E16) neonate. Right: epithelial cell hyperplasia in alveoli and a bronchiole from a *SOPten*$^{flox/flox}$(E10–E16) neonate. Scale bars: 50 μm. (**C**) Increased total cell numbers in lungs. Total cells from WT(E10–E16) and *SOPten*$^{flox/flox}$(E10–E16) lungs at P0 were counted. Data are expressed as the mean total lung cells ± SD for 4 mice/group. *$P < 0.05$, Student's *t* test. (**D**) Histological analysis of lungs at various embryonic stages. Lung sections were prepared from *SOPten*$^{flox/flox}$(E10–E16) mice at the indicated gestational stages and stained with H&E. Representative sections from WT(E10–E16) and *SOPten*$^{flox/flox}$(E10–E16) embryos are shown. No differences were detected between the WT and mutant embryos at E14.5 or E16.6, but dramatic differences were visible from E17.5 onward. WT(E10–E16) lungs showed dilatation of distal tubules and mesenchyme thinning at E17.5, with progression of septation from E17.5 to P0. *SOPten*$^{flox/flox}$(E10–E16) lungs showed fewer saccular structures during this period. Scale bars: 200 μm.

result of increases in the number and size of alveolar epithelial cells as well as elevated numbers of myofibroblast precursors in the septa. These defects in the blood-air barrier are likely responsible for the respiratory failure of *SOPten*$^{flox/flox}$(E10–E16) mice.

Impaired alveolar epithelial cell differentiation in SOPten$^{flox/flox}$*(E10–E16) embryos.* Bronchioalveolar epithelial cells differentiate during the terminal sac stage, resulting in distinct cell lineages generated along a proximodistal axis (20). To determine the level of maturity of alveolar epithelial cells in *SOPten*$^{flox/flox}$(E10–E16) lungs, we examined the expression of lung epithelial cell–specific marker proteins by Western blotting and IHC analysis. The expression levels of the AE-II cell marker surfactant proteins A (SP-A), -B, -C, and -D as well as that of the AE-I cell marker aquaporin-5 (AQP5) were severely attenuated in *SOPten*$^{flox/flox}$(E10–E16) lungs compared with WT(E10–E16) lungs at E19.5 (Figure 2, B and C). The defect in alveolar epithelial cell differentiation in *SOPten*$^{flox/flox}$(E10–E16) lungs was confirmed by transmission electron microscopy. In WT(E10–E16) lungs at E19.5, AE-I cells are distinctive in appearance and characterized by their squamous morphology. WT AE-II cells are recognized by their characteristic apical microvilli and lamellar bodies, which are involved in the storage and exocytosis of SPs (Figure 2A, lower left panel). In addition, surfactant materials are observed within the saccular spaces of WT(E10–E16) lungs (Figure 2A, arrow). In contrast, the septa in the *SOPten*$^{flox/flox}$(E10–E16) mice contained many immature alveolar epithelial cells, i.e., rounded to cuboidal cells having poorly differentiated cytoplasm, rare apical microvilli, and few lamellar bodies (Figure 2A, lower right panel). These mutant cells were also positive for PAS staining at P0 (data not shown), in contrast to the negative PAS staining of differentiated WT(E10–E16) alveolar epithelial cells (26). The defect in cell differentiation was restricted to alveolar epithelial cells because the expression levels of Clara cell secretory protein (CCSP, a Clara cell marker; Figure 2, B and C) and calci-

Table 2
SOPten$^{flox/flox}$ (E10–E16) mice show hypoxia

	WT(E10–E16)	*SOPten*$^{flox/flox}$(E10–E16)	*P*
pH	7.44 ± 0.04	6.89 ± 0.19	0.0083
PaO_2 (Torr)	106.4 ± 4.6	57.6 ± 3.5	0.001
$PaCO_2$ (Torr)	38.4 ± 4.6	72.5 ± 20.8	0.04
SaO_2(%)	100.0 ± 0.0	48.7 ± 12.2	0.0003

Arterial blood gas analysis in WT(E10–E16) and *SOPten*$^{flox/flox}$(E10–E16) mice at P0. Results are expressed as the mean ± SD of 4 mice/group. Statistical differences were determined using the Student's *t* test.

tonin gene–related peptide (CGRP, a neuroendocrine cell marker; Figure 2C) were similar in WT(E10–E16) and *SOPten*$^{flox/flox}$(E10–E16) lungs. Furthermore, the development of the proximal epithelium appeared normal because ciliated cells were observed both in WT(E10–E16) and *SOPten*$^{flox/flox}$(E10–E16) lungs (data not shown). These results show that loss of Pten in utero affects distal alveolar epithelial cell differentiation during lung development. The reduction in the production of SPs caused by impaired alveolar epithelial cell differentiation may contribute to the respiratory failure of *SOPten*$^{flox/flox}$(E10–E16) embryos.

Defective expression of molecular markers in SOPten$^{flox/flox}$*(E10–E16) embryos.* To examine the expression of key molecules involved in lung morphogenesis and distal epithelial cell differentiation, we performed RT-PCR analyses of whole lung tissue from E19.5 WT(E10–E16) and *SOPten*$^{flox/flox}$(E10–E16) embryos. The expression of Spry2, a Sprouty family protein that negatively regulates lung morphogenesis and SP-A, -B, and -C expression in murine embryonic lungs (27, 28), and Shh, a soluble factor that positively regulates epithelial and mesenchymal cell proliferation during lung development (29, 30), were dramatically upregulated in *SOPten*$^{flox/flox}$(E10–E16) lungs (Figure 3A). There were no differences between the genotypes in the expression of signaling molecules such as FGFs, bone morphogenetic protein, and Wnt7b, or in various transcription factors important for alveolar epithelial cell differentiation. Immunostaining of *SOPten*$^{flox/flox}$(E10–E16) lungs with anti-Spry2 and anti-Shh antibodies revealed markedly elevated expression of these molecules compared with their levels in WT(E10–E16) lungs, especially in mutant alveolar epithelial cells (Figure 3B). These data suggest that abnormally increased expression of Spry2 and Shh in alveolar epithelial cells may underlie the impaired alveolar epithelial cell differentiation and epithelial and mesenchymal cell proliferation seen in *SOPten*$^{flox/flox}$(E10–E16) mice.

Bronchioalveolar epithelial hyperplasia and increased cell size of alveolar epithelial cells in postnatal SOPten$^{flox/flox}$ *mice.* To determine whether mice that suffered loss of Pten after birth develop lung tumors, we administered doxycycline to WT and *SOPten*$^{flox/flox}$ mice at P21 or P84 for 7 days and examined the bronchioalveolar epithelium 9 weeks later. Histological analysis revealed mild bronchiolar and alveolar epithelial hyperplasia in both *SOPten*$^{flox/flox}$(P21–P27) and

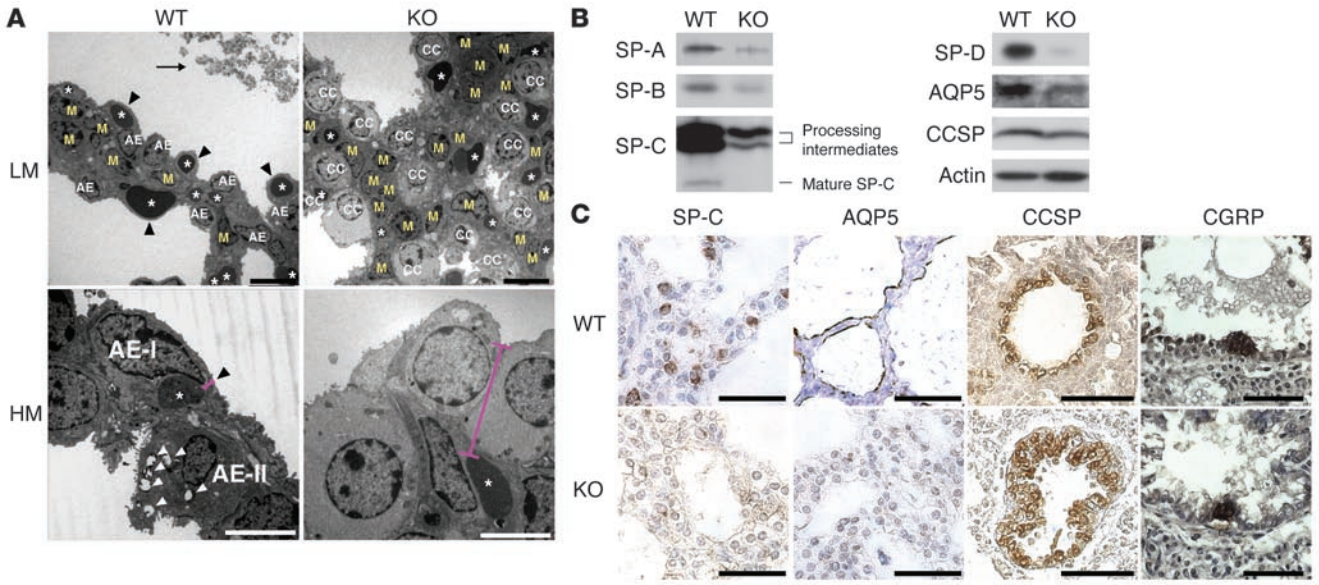

Figure 2
Abnormal thickness of the blood-air barrier and impaired alveolar epithelial cell differentiation in *SOPten*$^{flox/flox}$(E10–E16) lungs. (**A**) Transmission electron micrographs of the lung septa of E19.5 embryos shown at low (LM) and high (HM) magnification. WT(E10–E16) lung showed AE-I and AE-II cells plus 2 layers of capillaries (asterisks) separated by mesenchymal cells (M; upper left panel). The AE-II cells contained many lamellar bodies (white arrowheads) and apical microvilli (lower left panel). SPs (arrow) were visible in the saccular spaces (upper left panel). Black arrowheads (left panels) indicate the thin, normal blood-air barrier, composed of AE-I cells and capillary endothelial cells, in the WT lung. In the *SOPten*$^{flox/flox}$(E10–E16) lung, the septa were thick with increased mesenchymal cells (upper right panel). Increased numbers of undifferentiated cuboidal epithelial cells of enlarged size were present (CC; upper right panel). The blood-air barrier (red bars) was significantly thicker in *SOPten*$^{flox/flox}$ lungs than in WT lungs (lower panels). Scale bars: 10 μm (LM); 5 μm (HM). (**B** and **C**) Altered marker protein expression. (**B**) Western blotting of SP-A, -B, -C, -D, AQP5, and CCSP proteins in extracts of whole lungs taken from WT(E10–E16) and *SOPten*$^{flox/flox}$(E10–E16) mice at E19.5. Actin was used as a loading control. Data shown are representative of 3 trials. (**C**) IHC analysis of SP-C, AQP5, CCSP and CGRP. SP-C and AQP5 immunostaining was intense in cuboidal AE-II and flat AE-I cells, respectively, in WT(E10–E16) lungs at E19.5 but dramatically decreased in *SOPten*$^{flox/flox}$(E10–E16) lung at E19.5. Scale bars: 50 μm.

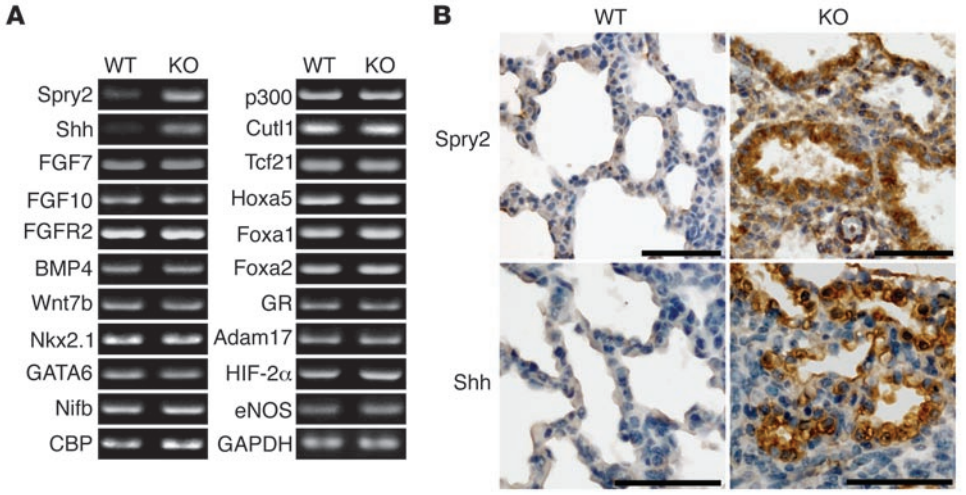

Figure 3
Altered gene expression profile during lung morphogenesis and distal epithelial cell differentiation in *SOPten*$^{flox/flox}$(E10–E16) lungs. (**A**) RT-PCR analyses of the mRNA expression of the indicated genes in lungs of WT(E10–E16) and *SOPten*$^{flox/flox}$(E10–E16) mice at E19.5. Spry2 and Shh are differentially expressed. GAPDH was used as a loading control. Data shown are representative of 3 trials. (**B**) IHC analysis of Spry2 and Shh expression in lungs of WT(E10–E16) and *SOPten*$^{flox/flox}$(E10–E16) mice at E19.5. A dramatic upregulation of Spry2 and Shh in the alveolar epithelium in *SOPten*$^{flox/flox}$(E10–E16) lungs was observed. Scale bars: 50 μm.

SOPten$^{flox/flox}$(P84–P90) mice (Figure 4A). However, the structure of these alveolar epithelial cells in *SOPten*$^{flox/flox}$(P21–P27) and *SOPten*$^{flox/flox}$(P84–P90) mice was normal, as determined by transmission electron microscopy (Figure 4B). An increase in the cell size of both AE-I and AE-II cells was also evident in both *SOPten*$^{flox/flox}$(P21–P27) and *SOPten*$^{flox/flox}$(P84–P90) lungs (Figure 4B). IHC analyses of lung epithelial cell–specific marker proteins showed no significant differences in bronchiolar and alveolar epithelial differentiation in *SOPten*$^{flox/flox}$(P21–P27) and *SOPten*$^{flox/flox}$(P84–P90) mice compared with controls (Figure 4C).

Spontaneous lung adenocarcinomas and increased susceptibility to urethane-induced lung tumor formation in SOPten$^{flox/flox}$ *mice*. About 10% of *SOPten*$^{flox/flox}$(E10–E16) mice survived until adulthood. Because a reduction or absence of PTEN protein expression has frequently been reported in human non–small cell lung cancers, we monitored 14 *SOPten*$^{flox/flox}$(E10–E16) mice and 48 WT(E10–E16) mice for 90 weeks after birth to analyze the effect of Pten deficiency on lung tumor onset. Strikingly, all *SOPten*$^{flox/flox}$(E10–E16) mice showed macroscopic lung tumors (Supplemental Figure 4A, upper right panel). Histological examination revealed that 13 of these tumors were adenocarcinomas (Supplemental Figure 4A, lower left panel), while 1 mutant mouse developed a squamous cell carcinoma (Supplemental Figure 4A, lower right panel). In contrast, spontaneous lung tumor formation was not observed in any WT(E10–E16) mice (Supplemental Figure 4A, upper left panel) during the observation period. Kaplan-Meier analyses showed that the cancer-free survival rates for *SOPten*$^{flox/flox}$(E10–E16) mice were significantly lower than for controls (log-rank, $P < 0.001$; Supplemental Figure 4B).

We next investigated the effect of Pten deficiency on carcinogenesis in the lung after this organ had been fully formed. As was true for *SOPten*$^{flox/flox}$(E10–E16) mice, 87% (13/15) of *SOPten*$^{flox/flox}$(P21–P27) mice showed spontaneous lung adenocarcinoma formation, whereas no tumors were observed in WT(P21–P27) lungs ($n = 36$) during the 40- to 70-week observation period (Figure 5A). These findings indicate that Pten function is essential both prenatally and postnatally for preventing lung tumorigenesis, especially the development of adenocarcinomas.

To examine chemically induced lung carcinogenesis in the absence of Pten, 8- to 10-week-old WT(E10–E16) and *SOPten*$^{flox/flox}$(E10–E16) mice were i.p. injected with urethane, a well known initiator of lung carcinomas (31). At 20 weeks after injection, lung tumors had developed in 94% (17/18) of *SOPten*$^{flox/flox}$(E10–E16) mice, whereas only 42% (11/26) of WT(E10–E16) animals showed lung tumors ($P < 0.001$). The numbers and sizes of the lung tumors were also significantly greater in *SOPten*$^{flox/flox}$(E10–E16) mice than in WT(E10–E16) mice (Supplemental Figure 4C, upper panels, and Supplemental Figure 4D). Histological examination demonstrated that 1 *SOPten*$^{flox/flox}$(E10–E16) mouse developed a lung adenocarcinoma (Supplemental Figure 4C, lower right panel), whereas all other tumors that formed in both WT and *SOPten*$^{flox/flox}$ lungs were lung adenomas (Supplemental Figure 4C, lower left panel). Similar results were obtained when the lungs of WT(P21–P27) and *SOPten*$^{flox/flox}$(P21–P27) mice were subjected to urethane treatment. The numbers and sizes of the tumors that developed in the lungs of *SOPten*$^{flox/flox}$(P21–P27) mice were significantly greater than those forming in WT(P21–P27) lungs ($P < 0.001$ and $P < 0.005$, respectively; Figure 5, B and C). Thus, both prenatal and postnatal Pten-deficient mice show increased susceptibility to urethane-induced lung tumorigenesis.

Pten deficiency induces significant increases in numbers of BASCs and side population cells. Our results showed that bronchioalveolar epithelium–specific Pten deficiency almost inevitably leads to lung adenocarcinoma. Since lung adenocarcinomas reportedly originate from BASCs, which are defined as Sca-1$^+$CD45$^-$CD31$^-$CD34$^+$ and possess stem cell properties (5), we evaluated the number of BASCs present in lungs of WT(P21–P27) and *SOPten*$^{flox/flox}$(P21–P27) mice prior to the development of tumors in the latter. Interestingly, there was a 5.2-fold increase in BASCs in 8-week-old *SOPten*$^{flox/flox}$(P21–P27) mice compared with WT(P21–P27) animals ($P < 0.05$, Figure 6A and 6B, right panel). A comparable increase in BASCs was observed in *SOPten*$^{flox/flox}$(E10–E16) mice compared with WT(E10–E16) mice ($P < 0.05$; Figure 6B, left panel). We also examined the lungs of WT(P21–P27) and *SOPten*$^{flox/flox}$(P21–P27) mice for side population cells, which exhibit Hoechst dye efflux properties commonly observed in various types of stem cells (32). The side population fraction is highly enriched in clonogenic cells of the proximal and distal airway (including BASCs; ref. 33) that express epithelial transcription factors (34). In lungs of 8-week-old *SOPten*$^{flox/flox}$(P21–P27) mice, we found a 4.0-fold increase in side population cells compared with controls ($P < 0.005$; Figure 6,

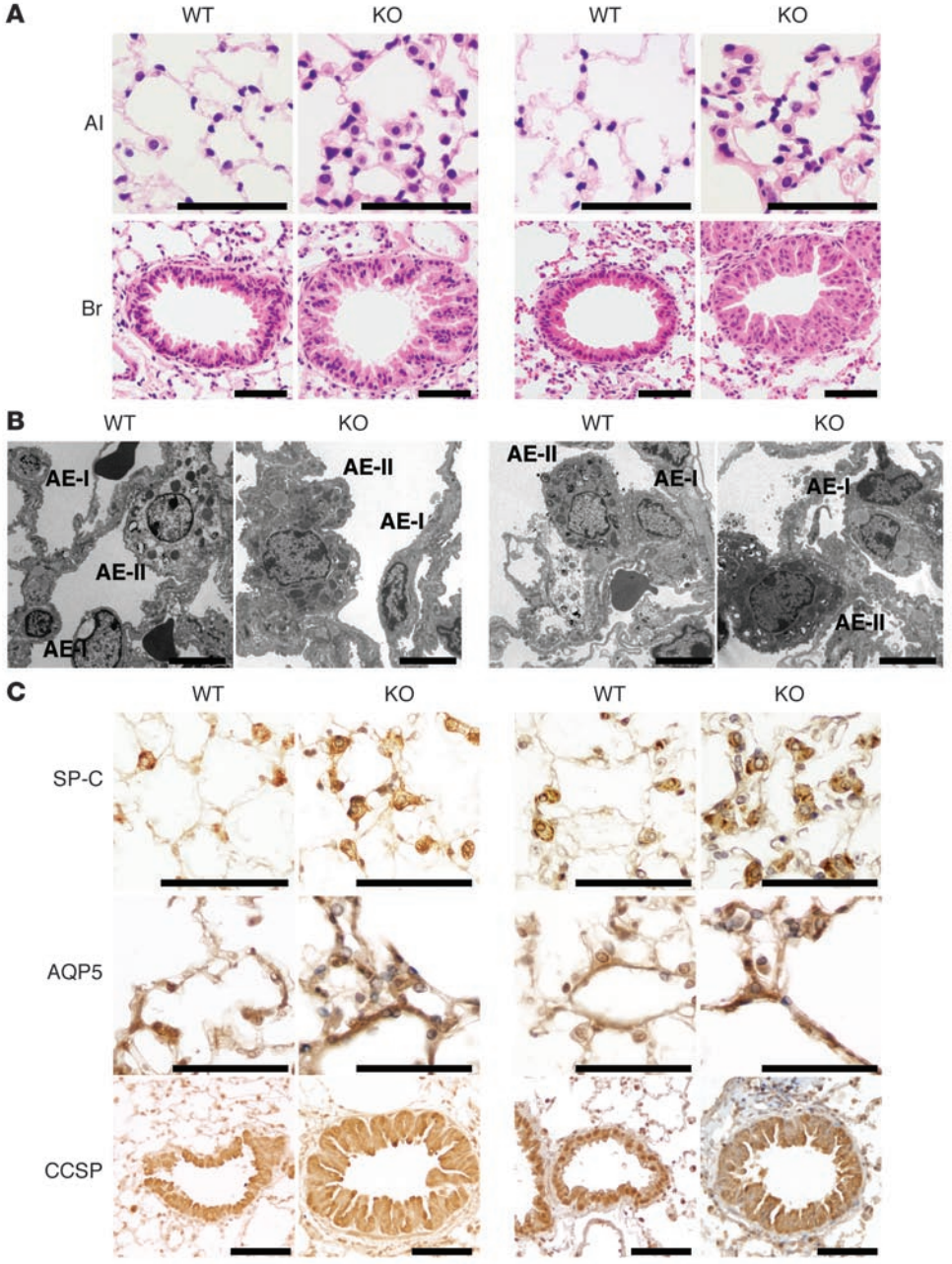

Figure 4
Bronchiolar and alveolar epithelial cell hyperplasia and increased cell size in *SOPten*$^{flox/flox}$ mice that received doxycycline postnatally. (**A**) Histologic analyses of lungs from WT(P21–P27) and *SOPten*$^{flox/flox}$(P21–P27) and WT(P84–P90) and *SOPten*$^{flox/flox}$ (P84–P90) mice. Mild epithelial cell hyperplasia in alveoli and a bronchiole could be observed at both time points. Scale bars: 50 μm. (**B**) Transmission electron micrographs of the lung septa from WT(P21–P27) and *SOPten*$^{flox/flox}$(P21–P27) and WT(P84–P90) and *SOPten*$^{flox/flox}$ (P84–P90) mice. The increased sizes of AE-I and AE-II cells can be seen in *SOPten*$^{flox/flox}$ lungs at both time points. Lamellar bodies and apical microvilli, which are signature structures of AE-II cells, are visible within the AE-II cells of both WT and *SOPten*$^{flox/flox}$ lungs. Scale bars: 5 μm. (**C**) IHC analysis of SP-C, AQP5, and CCSP expression in lungs of WT(P21–P27) and *SOPten*$^{flox/flox}$(P21–P27) mice (left panels) and WT(P84–P90) and *SOPten*$^{flox/flox}$(P84–P90) mice (right panels). Although the numbers of AE-I and AE-II cells were increased in lungs of *SOPten*$^{flox/flox}$(P21–P27) and *SOPten*$^{flox/flox}$(P84–P90) mice, no significant differences between WT and *SOPten*$^{flox/flox}$ mice were observed in the staining intensity of SP-C, AQP5, or CCSP at either time point. Scale bars: 50 μm.

C and D, right panel). Lung side population cells were similarly increased in *SOPten*$^{flox/flox}$(E10–E16) mice compared with WT(E10–E16) mice ($P < 0.05$; Figure 6D, left panel). These results indicate that Pten deficiency leads to an abnormal increase in numbers of BASCs and side population cells.

Altered cancer-related molecules in SOPten$^{flox/flox}$ *lungs*. Several downstream effectors of the Pten/PI3K pathway are reportedly involved in stem cell self renewal and lung carcinogenesis (15, 35–41). We used Western blotting to examine the expression of these molecules in whole lung extracts from 8-week-old WT(P21–P27) and *SOPten*$^{flox/flox}$(P21–P27) mice. Phosphorylation levels of Akt were significantly elevated in the mutant lungs (Figure 7A). In addition, *SOPten*$^{flox/flox}$(P21–P27) lungs showed increased expression of c-Myc, Bcl-2, and Shh but decreased expression of p27 (Figure 7A). Parallel molecular alterations were observed in the lungs of neonatal *SOPten*$^{flox/flox}$(E10–E16) mice (data not shown). There were no obvious differences between WT and *SOPten*$^{flox/flox}$ lungs (either prenatal or postnatal) in the expression of pErk, pRb, p53, p21, or Notch1. Among these molecules, activation of Akt (35), c-Myc (36), Shh (37), and Bcl-2 (38) and inactivation of p27 (39) have been shown to positively regulate stem cell self renewal. Moreover, elevated expression levels of pAkt (15), c-Myc (40), and Bcl-2 (41) have been observed in human lung adenocarcinomas. These findings collectively suggest that loss of Pten mediates alterations in the expression of molecules that promote the expansion of BASCs. This expansion may be an underlying cause of the onset of bronchioalveolar epithelial cell hyperplasia and lung adenocarcinomas observed in our Pten-deficient mutants.

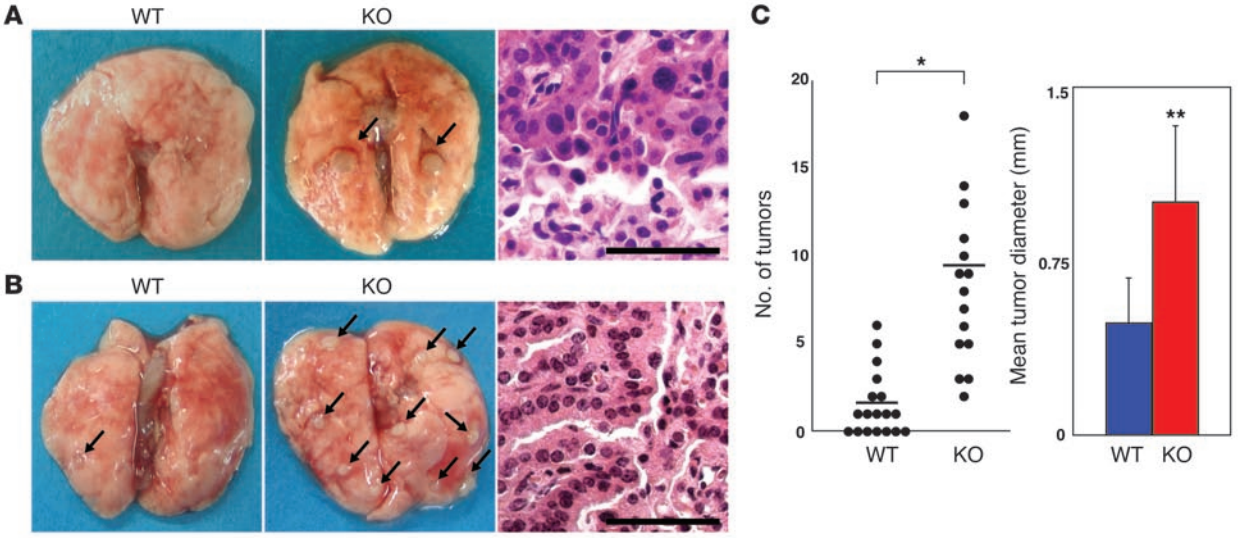

Figure 5
Spontaneous lung adenocarcinomas and urethane-induced lung tumors in *SOPten*$^{flox/flox}$ mice that received doxycycline postnatally. (**A**) Gross and histological analyses of spontaneous adenocarcinomas. Left and middle: gross appearance of a healthy lung in a 48-week-old WT(P21–P27) mouse and representative lung adenocarcinomas (arrow) in a lung of a 48-week-old *SOPten*$^{flox/flox}$(P21–P27) mouse. Right: histology of a spontaneous lung adenocarcinoma in the lung of a 48-week-old *SOPten*$^{flox/flox}$(P21–P27) mouse, representative of adenocarcinomas observed in 13/15 of these mice. Scale bar: 50 μm. (**B**) Gross and histological analyses of urethane-induced tumors. WT(P21–P27) (n = 18) and *SOPten*$^{flox/flox}$(P21–P27) mice (n = 15) were injected i.p. with urethane. After 20 weeks, the number of tumors and their diameters were measured from the lung surface. Left and middle: gross appearance of urethane-induced lung tumors (arrows) in WT(P21–P27) and *SOPten*$^{flox/flox}$(P21–P27) mice. Right: histology of a lung adenoma representative of those observed in both WT(P21–P27) and *SOPten*$^{flox/flox}$(P21–P27) mice. Scale bar: 50 μm. (**C**) Numbers and mean size of urethane-induced tumors in WT(P21–P27) and *SOPten*$^{flox/flox}$(P21–P27) mice. Horizontal bars in the left panel represent the mean tumor numbers for the WT(P21–P27) and *SOPten*$^{flox/flox}$(P21–P27) groups. The right panel shows the mean diameter ± SD of tumors in WT(P21–P27) and *SOPten*$^{flox/flox}$(P21–P27) lungs. *P < 0.001; **P < 0.005, Welch's t test.

Frequent K-ras mutations in spontaneous adenocarcinomas of SOPten$^{flox/flox}$*(P21–P27) lungs*. Because activating *K-ras* mutations are detected in 20%–30% of human lung adenocarcinomas (42), we hypothesized that the Pten deficiency in our mice might elevate the risk of additional oncogenic events such as *K-ras* mutations. We used direct sequencing of PCR-amplified DNAs to analyze paired samples of a spontaneous adenocarcinoma and the corresponding non-tumorous lung tissue from 6 *SOPten*$^{flox/flox}$(P21–P27) mice. Interestingly, activating point mutations in codon 61 of *K-ras* were observed in 2 of these 6 (33%) spontaneous adenocarcinomas. In both cases, the mutation was a transversion of the second nucleotide of codon 61 (CAA to CTA and CAA to CGA) (Figure 7B and data not shown). These types of alterations have been previously reported in spontaneous lung adenocarcinomas of A/J × C3H F1 mice (43). In contrast, no *K-ras* mutations were detected in the corresponding non-tumorous lung tissue samples obtained from the same *SOPten*$^{flox/flox}$(P21–P27) mice. Our results thus suggest that the expansion of BASCs driven by the loss of Pten in *SOPten*$^{flox/flox}$ mice may increase the risk of additional oncogenic mutations in these cells, including alterations of *K-ras*. The combined effects of Pten deficiency, *K-ras* mutation, and perhaps other tumorigenic events may further increase the proliferation of BASCs such that they eventually initiate lung adenocarcinoma formation.

Discussion

Pten is essential for lung morphogenesis and distal lung epithelial cell differentiation. The formation of the fetal lung occurs via a process of branching morphogenesis and depends upon complex paracrine signaling between epithelial and mesenchymal cells. This signaling in turn controls transcriptional programs regulating cell behavior during development (20). In this study, we provide what is to our knowledge the first evidence of a critical role for Pten in murine lung development. Targeted inactivation of the *Pten* gene in the embryonic pulmonary epithelium resulted in alveolar septal and bronchiolar hyperplasia, impairments of branching morphogenesis and distal alveolar epithelial cell differentiation, and, ultimately, failure of lung function.

Spatiotemporal localization of *Pten* gene expression has been previously reported in developing mice (21). High levels of Pten expression and low levels of Akt activation were observed in terminal sac–stage respiratory epithelium, whereas high levels of Akt activation and low levels of Pten expression occurred in the pseudoglandular stage (21, 44). Taken together with our finding that *SOPten*$^{flox/flox}$(E10–E16) mice show impairments of both terminal sac formation and alveolar epithelial cell differentiation, these observations demonstrate that Pten has an important role in lung development, especially during the terminal sac stage.

Lungs of *SOPten*$^{flox/flox}$(E10–E16) mice exhibited septal hyperplasia due not only to increased numbers of alveolar epithelial cells and mesenchymal cells (mainly myofibroblast precursors) but also to an enlargement of individual alveolar epithelial cells. These alterations led to a dramatic thickening of the blood-air barrier and inhibited efficient gas exchange. Because loss of Pten in various tissues activates Akt, which is important for cell proliferation and survival (45) and cell size regulation (46), the observed changes to the activation of Akt and its downstream effectors may account for the hyperproliferation and enlargement of Pten-deficient alveolar epithelial cells. The proliferation

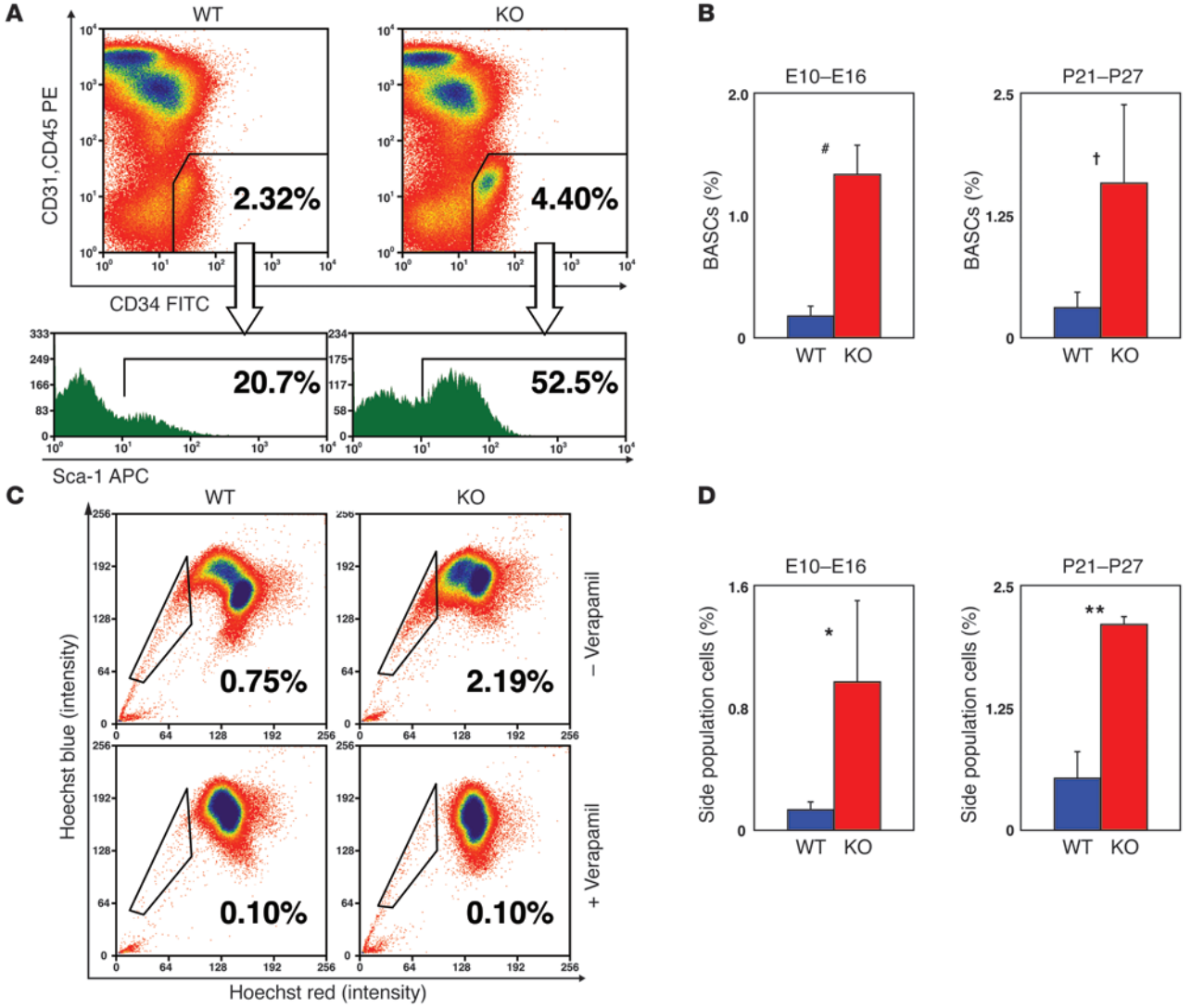

Figure 6

Pten deficiency induces significant increases in numbers of BASCs and side population cells. (**A**) Increased numbers of BASCs in lungs of *SOPten*$^{flox/flox}$(P21–P27) mice. Representative flow cytometric profiles of BASCs in lungs of 8-week-old WT(P21–P27) and *SOPten*$^{flox/flox}$(P21–P27) mice. Upper panels show the percentages of CD34$^+$CD45$^-$CD31$^-$ cells in the total lung cell population. Lower histograms show the percentages of Sca-1$^+$ cells in the CD34$^+$CD45$^-$CD31$^-$ population. (**B**) Bar graph representation of the percentages of BASCs in total lung cells of WT(E10–E16) and *SOPten*$^{flox/flox}$(E10–E16) mice and WT(P21–P27) and *SOPten*$^{flox/flox}$(P21–P27) mice. Data are expressed as the mean percentage ± SD for 4 mice/group. $^{\#}P = 0.011$; $^{\dagger}P = 0.015$. (**C**) Increased numbers of side population cells in *SOPten*$^{flox/flox}$(P21–P27) lungs. Representative flow cytometric profiles of side population cells in lungs of 8-week-old WT(P21–P27) and *SOPten*$^{flox/flox}$(P21–P27) mice. Side population cells were identified by staining with 5 μg/ml Hoechst 33342 alone (upper panels) or in combination with 50 μM verapamil, which is an inhibitor of ATP-binding cassette transporters and blocks the dye efflux (lower panels). The percentages of side population cells (boxed ares) in the total lung cells are indicated in each panel. (**D**) Bar graph representation of the percentages of side population cells in total lung cells of WT(E10–E16) and *SOPten*$^{flox/flox}$(E10–E16) and WT(P21–P27) and *SOPten*$^{flox/flox}$(P21–P27) mice. Data are expressed as the mean percentage of side population cells ± SD for 3 mice/group. $^*P < 0.05$; $^{**}P = 0.001$. For **B** and **D**, statistical differences were determined using the Student's *t* test. Data shown are representative of at least 4 trials.

of lung mesenchymal and alveolar epithelial cells is regulated by Pten as well as Shh, a soluble factor (29, 30). Overexpression of Shh in the distal airway epithelium causes increased proliferation of both mesenchymal and alveolar epithelial cells (29), and *Shh*-null mice show significantly reduced proliferation of these cell types (30). In our study, we detected a dramatic induction of Shh in the alveolar epithelium of *SOPten*$^{flox/flox}$(E10–E16) lungs compared with controls. Because activation of PI3K/Akt signaling upregulates Shh expression (47), the increased activation of the Shh pathway in *SOPten*$^{flox/flox}$(E10–E16) lung may be due to the enhanced PI3K/Akt signaling that occurs in the absence of Pten. The SP-C–Cre construct used to delete *Pten* in alveolar epithelial cells cannot delete the target gene in mesenchymal cells (23), meaning that Pten was likely intact in mesenchymal cells in our *SOPten*$^{flox/flox}$ mice. Indeed, our IHC study demonstrated that upregulation of Shh was confined to the alveolar

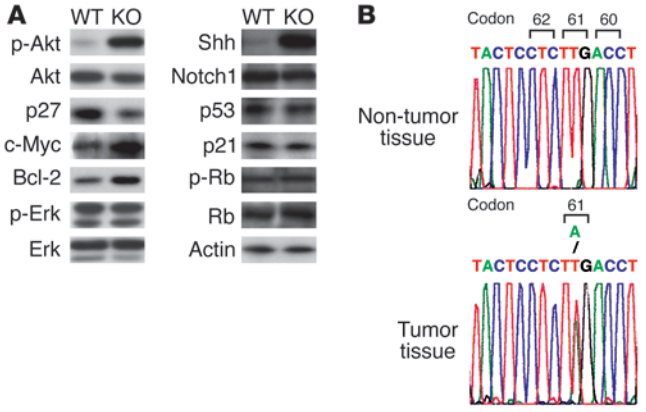

Figure 7
Altered cancer-related molecules in *SOPten*$^{flox/flox}$(P21–P27) lungs and identification of *K-ras* mutations in spontaneous lung adenocarcinomas of SOPten$^{flox/flox}$(P21–P27) mice. (**A**) Altered cancer-related molecules in *SOPten*$^{flox/flox}$(P21–P27) lungs. The phosphorylated forms of Akt, Erk1/2 and Rb and the expression of p27, c-Myc, Bcl-2, Notch1, Shh, p53 and p21 were detected by immunoblotting of lysates of whole lung tissue from 8-week-old WT(P21–P27) and *SOPten*$^{flox/flox}$(P21–P27) mice. Total Akt, total Erk, total Rb, and actin were evaluated as controls. Data shown are representative of 3 trials. (**B**) Identification of K-ras mutations in spontaneous lung adenocarcinomas of *SOPten*$^{flox/flox}$(P21–P27) mice. Top: Normal nucleotide sequence of codons 60–62 of the *K-ras* gene in the genomic DNA of non-tumorous tissue taken from *SOPten*$^{flox/flox}$(P21–P27) lungs. The antisense strand is shown for exon 2. Bottom: Detection of a T-to-A transversion at the second position of codon 61 in the genomic DNA of a spontaneous adenocarcinoma in *SOPten*$^{flox/flox}$(P21–P27) lung tissue. Data shown are representative of 3 trials.

epithelium and was not observed in mesenchymal cells. Thus the enhanced proliferation of mesenchymal cells observed in *SOPten*$^{flox/flox}$(E10–E16) mice might be caused by the elevated production of soluble Shh by Pten-deficient alveolar epithelial cells. The increased proliferation of alveolar epithelial cells may also result in part from enhanced Shh signaling and autocrine production of Shh.

The lungs of *SOPten*$^{flox/flox}$(E10–E16) mice at E19.5 showed rare apical microvilli, few lamellar bodies, PAS positivity, and reduced production of SPs. These observations suggest that Pten is involved in the maturation of AE-II epithelium. Because AE-I cells can be generated from AE-II cells (20), AE-I cell differentiation is also impaired in *SOPten*$^{flox/flox}$(E10–E16) lungs. Screening of the expression of 20 genes important in distal epithelial cell differentiation revealed a marked increase in Spry2 expression in Pten-deficient alveolar epithelium. Overexpression of Spry2 in the distal airway epithelium leads to decreased SP-C mRNA expression (28), and reduction of Spry2 expression by antisense oligonucleotides results in increased expression of SP-A, -B, and -C in the lung (27). Thus the enhanced expression of Spry2 by the alveolar epithelium of *SOPten*$^{flox/flox}$(E10–E16) lungs may be responsible (at least in part) for the observed defect in AE-II cell differentiation. Since insufficient secretion of SPs by AE-II cells is a major cause of respiratory distress syndrome in mammalian neonates (26), the neonatal lethality of *SOPten*$^{flox/flox}$(E10–E16) mice may be caused not only by the thickened blood-air barrier but also by impaired AE-II differentiation. Collectively, our data provide novel molecular evidence of a previously unrecognized contribution of Pten to normal lung morphogenesis and alveolar epithelial cell differentiation.

In contrast to *SOPten*$^{flox/flox}$(E10–E16) mice, *SOPten*$^{flox/flox}$(P21–P27) and *SOPten*$^{flox/flox}$(P84–P90) mice examined at 9 weeks after doxycycline administration showed no significant difference in alveolar epithelial differentiation compared with WT(P21–P27) or WT(P84–P90) mice. Specifically, the expression levels of SP-C and AQP5 in *SOPten*$^{flox/flox}$(P21–P27) and *SOPten*$^{flox/flox}$(P84–P90) lungs were essentially comparable with those in the WT(P21–P27) and WT(P84–P90) controls, respectively, although the mild alveolar epithelial hyperplasia and increased cell size observed in *SOPten*$^{flox/flox}$(E10–E16) mice were also seen in both *SOPten*$^{flox/flox}$(P21–P27) and *SOPten*$^{flox/flox}$(P84–P90) mice. These discrepant effects of Pten deficiency on alveolar epithelial differentiation in *SOPten*$^{flox/flox}$(E10–E16) mice versus *SOPten*$^{flox/flox}$(P21–P27) and *SOPten*$^{flox/flox}$(P84–P90) mice may be explained in 2 ways. First, since the turnover time of the respiratory epithelia of adult rodents is reported to be greater than 16 weeks (48), differentiated epithelial cells that were present prior to doxycycline administration to *SOPten*$^{flox/flox}$(P21–P27) or *SOPten*$^{flox/flox}$(P84–P90) mice may have survived. Second, since AE-II cells and Clara cells have proliferative capacity in adult mice (2), and AE-I cells can be generated from AE-II cells (20), Pten deficiency in the mouse lung may increase the proliferation and/or survival of these committed cells as well as increase their size.

Pten deficiency leads to increased BASC numbers and lung adenocarcinomas. In this study we demonstrated that almost all mice with a bronchioalveolar-specific Pten deficiency spontaneously developed lung adenocarcinomas. In both *SOPten*$^{flox/flox}$(P21–P27) and *SOPten*$^{flox/flox}$(E10–E16) mice, the lungs showed increased numbers of both BASCs and stem cell–like side population cells. Two lines of evidence suggest that BASCs initiate lung adenocarcinomas. First, lung injury induces an increase in BASCs that correlates positively with both the incidence and size of lung adenocarcinomas (5). Second, the BASC population is expanded in tissues that subsequently develop lung tumors in vivo (5). Cancers of diverse tissues are thought to be maintained by minor subpopulations of cells within the tumor called cancer stem cells (4), and BASC-like cells have been detected in established adenocarcinomas (49). Therefore, BASCs may not only initiate tumors but may also function as cancer stem cells, driving tumor development and progression, similar to cancer stem cells observed in hematopoietic (50), breast (51), and brain (52) malignancies. Because BASCs are increased in the lungs of *SOPten*$^{flox/flox}$ mice, these animals have a greater risk of acquiring multiple oncogenic mutations and developing cancer. Indeed, the tumors observed in *SOPten*$^{flox/flox}$ lungs (which show increased BASC numbers) are much more frequent and larger than those in WT lungs and also show frequent mutation of the *K-ras* oncogene. The facts that Pten deletion leads to stem and/or progenitor cell expansion in the prostate (10), central nervous system (9), and blood cells (11) and promotes the generation of leukemia-initiating cells (11) support our hypothesis.

Significantly, almost all *SOPten*$^{flox/flox}$ mice in which Pten was deleted post-natally also developed spontaneous adenocarcinomas. Previous studies reported that somatic inactivation of PTEN in human lung tumors makes an important contribution to the progression of established human lung cancers (53). In contrast, our experimental model indicates that postnatal loss of Pten function can actually initiate lung tumors in mice. In

combination, these findings demonstrate that Pten has a key role in preventing lung adenocarcinoma formation and blocking the progression of these malignancies.

To date, the only molecule that has been reported to affect BASC numbers is K-ras. Overexpression of K-ras increases both BASC numbers and the incidence of lung adenocarcinomas in mice (5). Our Western blotting assay revealed no significant differences between WT(P21–P27) and *SOPten*$^{flox/flox}$(P21–P27) lungs in the activation of Erk, a downstream effector of K-ras. Therefore, K-ras may not be involved in the process that enhances BASC numbers in non-tumorous regions of *SOPten*$^{flox/flox}$(P21–P27) lungs. However, we found that *K-ras* mutation had occurred in one-third of lung adenocarcinoma samples obtained from *SOPten*$^{flox/flox}$(P21–P27) mice, whereas no mutation was detected in the paired non-tumorous lung samples of the same mice. It is possible that the occurrence of a *K-ras* mutation in Pten-deficient BASCs may further increase BASC proliferation and eventually induce the formation of lung adenocarcinomas.

The onset of skin tumor formation in mice requires Akt signaling in addition to SOS/Ras/ERK signaling (54). Indeed, the MAPK/ERK pathway has been reported to act in synergy with the PI3K pathway to stimulate cyclin D1 transcription in NIH3T3 cells (55). Thus the onset of tumors in *SOPten*$^{flox/flox}$ mice could be caused principally by BASC hyperproliferation and/or apoptotic resistance induced by PI3K and Akt hyperactivation, with a contribution by deregulated ERK activation. The spatiotemporal relationship between loss of PTEN and mutation of *K-ras* has not been elucidated in human lung tumors. However, considering that loss of PTEN expression (14, 15) is much more frequent than *K-ras* mutation (42) in human lung adenocarcinomas, PTEN deficiency (rather than *K-ras* mutation) may be the primary event driving human lung adenocarcinoma development.

Our study also provides insight into the molecular mechanism underlying the increase in BASC numbers and adenocarcinoma onset in Pten-deficient mice. Loss of Pten in the lung leads not only to activation of Akt but also to elevated expression of c-Myc, Bcl-2, and Shh and decreased expression of p27. These gene expression alterations have been shown to induce stem cell self renewal and/or progenitor cell expansion and to trigger tumor formation in a variety of organs (15, 35–41). Significantly, c-Myc, Bcl-2, Shh, and p27 are all downstream targets of Akt (47, 56, 57). Our data therefore suggest that the increased BASC numbers and adenocarcinoma formation in *SOPten*$^{flox/flox}$ mice are likely due to the enhanced Akt activation that occurs in the absence of Pten.

Our study is, to our knowledge, the first report of a functional analysis of Pten in murine bronchioalveolar cells in vivo. We have demonstrated that an intact PI3K/Pten/Akt pathway in bronchioalveolar cells is essential for normal lung morphogenesis and BASC homeostasis as well as for the prevention of lung tumorigenesis. Our results suggest that the PI3K/PTEN/Akt pathway, particularly in BASCs and/or cancer stem cells, may be an attractive therapeutic target for the treatment of lung adenocarcinomas in humans.

Methods

Generation of SOPten$^{flox/flox}$ *mice and doxycycline administration*. *Pten*$^{flox/flox}$ mice (129Ola × C57BL6/J F6), generated as previously described (24), were mated to *SP-C-rtTA* mice (23) that expressed the rtTA gene (23) (which can be activated by doxycycline) under the control of the 3.7-kb human SP-C promoter. The human SP-C promoter selectively directs expression of the transgene in BASCs, in bronchioalveolar epithelial cells of primordial lung buds, and in both developing and mature bronchiolar and AE-II cells (58). Transgenic *(tetO)*$_7$*-Cre* mice (22), in which Cre expression is activated by rtTA, were mated to *SP-C-rtTA*/*Pten*$^{flox/flox}$ (*SPten*$^{flox/flox}$) mice to generate triple transgenic mice. Offspring carrying *SP-C-rtTA* and *(tetO)*$_7$*-Cre* plus 2 copies of the floxed *Pten* allele (*SOPten*$^{flox/flox}$) and offspring carrying *(tetO)*$_7$*-Cre* plus 2 copies of the floxed *Pten* allele (*OPten*$^{flox/flox}$) were used in the analysis as homozygous mutant (*SOPten*$^{flox/flox}$) and WT (*OPten*$^{flox/flox}$) mice, respectively. *SPten*$^{flox/flox}$ mice and *Pten*$^{flox/flox}$ mice were also used as WT controls in some experiments because *OPten*$^{flox/flox}$, *SPten*$^{flox/flox}$, and *Pten*$^{flox/flox}$ mice were indistinguishable in pilot experiments examining histology and Pten protein expression levels. To induce expression of the *Cre* transgene in BASCs, mice were administered doxycycline in utero or postnatally. Specifically, dams bearing pups (E10), 3-week-old mice (P21), and 12-week-old mice (P84) were fed doxycycline (Sigma-Aldrich) in their drinking water (1 mg/ml) for 7 days (23). After this period of doxycycline administration, the mice were designated as E10–E16, P21–P27, or P84–P90 mice, respectively. All animal experiments were approved by the Animal Experiment Review Board of the Akita University School of Medicine.

PCR analyses and Southern and Western blotting. Mouse genotyping was performed by PCR as previously described (59) using genomic DNA isolated from mouse tails. Sequences of the primers specific for the floxed *Pten* allele, WT *Pten* allele, and *SP-C-rtTA* and *(tetO)*$_7$*-Cre* transgenes are provided in Supplemental Table 1.

For Southern and Western blots, whole lung tissues were obtained from neonatal or 8-week-old WT and *SOPten*$^{flox/flox}$ mice that had been exsanguinated, perfused with 4°C PBS, and subjected to bronchioalveolar lavage with 4°C PBS to reduce hematocyte contamination. Genomic Southern blots of whole lung tissues were performed as described in ref. 59. Lysates of whole lung tissue (30 μg) were analyzed by Western blotting using antibodies recognizing the following proteins: Pten (Cascade Bioscience), phosphorylated Akt (Ser473), total Akt, phosphorylated Erk (Thr202/Tyr204), total Erk, and phosphorylated Rb (Ser807/811) (all from Cell Signaling Technology); total Rb, p27, c-Myc, p21, Bcl-2, Shh, Notch1, SP-A, SP-C, and AQP5 (all from Santa Cruz Biotechnology Inc.); p53 (DAKO); SP-B and SP-D (all from Chemicon International Inc.); CCSP (Upstate); and actin (Sigma-Aldrich).

Arterial blood gas analysis. Soon after birth, samples of arterial blood (80–100 μl) were collected from the carotid arteries of WT(E10–E16) and *SOPten*$^{flox/flox}$(E10–E16) mice at room temperature and immediately analyzed for blood gases on a blood gas analyzer (Radiometer ABL 510; Diamond Diagnostics).

Total cell number determinations in neonatal lungs. Lungs of neonatal mice were minced and treated with 1,000 U dispase (Godoshusei) for 15 minutes at 37°C and filtered using a Cell Strainer (Becton Dickinson — Discovery Labware). Dissociated lung cells were washed and resuspended in PBS, and the total cell number per lung was determined by Giemsa nuclear staining.

Histology and immunohistochemistry. Lungs were fixed in either 4% paraformaldehyde in PBS or Amsterdam's fixative (methanol/acetone/acetic acid/water, 35:35:5:25 v/v) and embedded in paraffin using standard procedures. Sections (5 μm) were mounted on slides for histological or IHC analysis. IHC analysis was performed using an indirect method with antibodies recognizing the following proteins: SP-C, AQP5, Spry2, Shh, and GFAP (all from Santa Cruz Biotechnology Inc.); CCSP (Upstate); CGRP (Sigma-Aldrich); CD31 (Pharmingen); and α-SMA and desmin (DAKO).

Electron microscopy. Lung tissues were washed with washing buffer (3.5% sucrose in 0.1 M sodium cacodylate buffer at pH 7.3), postfixed in buffered osmium tetroxide, and embedded in epoxy for electron microscopy according to the standard procedures. Ultrathin sections were stained in uranyl acetate plus lead citrate and examined using a 100CX electron microscope operated at 60 kV (JEOL Ltd).

RT-PCR. Total RNA from lung tissues of E19.5 WT(E10–E16) and *SOPten*$^{flox/flox}$(E10–E16) embryos was extracted using TRIzol (Invitrogen) according to manufacturer's protocol. Total RNA (5 μg) was reverse-transcribed using the Advantage RT-for-PCR kit (Cambrex). Sequences of specific primers are listed in Supplemental Table 1.

Cell proliferation and apoptosis. Cell proliferation was assessed using BrdU incorporation. Timed pregnant WT(E10–E16) and *SOPten*$^{flox/flox}$(E10–E16) mice at E19.5 were injected i.p. with 50 mg/kg body weight of BrdU (Sigma-Aldrich) in sterile PBS. After 2 hours, lungs of embryos were collected and fixed in 4% paraformaldehyde. Anti-BrdU staining was performed as described in ref. 60. For apoptosis, the frequency of apoptotic cells in the lungs of E19.5 embryos was determined by the TUNEL assay using the In Situ Cell Death Detection Kit (Roche Diagnostics GmbH) according to the manufacturer's protocol. Sections were counterstained with DAPI.

Tumor induction by urethane. *SOPten*$^{flox/flox}$(E10–E16) (n = 18) and *SOPten*$^{flox/flox}$ (P21–P27) (n = 15) mice, as well as their littermate controls WT(E10–E16) (n = 26) and WT(P21–P27) (n = 18), were injected i.p. at 8–10 weeks of age with 1 mg/g body weight urethane (Sigma-Aldrich) in PBS as previously described (31). At 20 weeks following urethane injection, mice were sacrificed and their lungs dissected. Lung tumor numbers and sizes were evaluated under a dissecting microscope, and individual tumors were examined histologically.

Flow cytometric analyses of BASCs and side population cells. Single-cell suspensions were prepared from lungs that were exsanguinated and perfused with PBS as described previously (5). Lung cells were resuspended in PBS/10% FCS at 2 × 10^6/100 μl and stained with APC-conjugated anti–Sca-1, PE-conjugated anti-CD45.1, FITC-conjugated anti-CD34 (all from eBioscience), and PE-conjugated anti-CD31 (Pharmingen). For analysis of side population cells, Hoechst staining was used as previously described (34). After Hoechst staining, cells were stained with PE-conjugated anti-CD31, PE-conjugated anti-CD4, PE-conjugated anti-CD8, PE-conjugated anti-CD11b, and PE-conjugated anti–Gr-1 (all from Pharmingen) to separate epithelial cells from endothelial cells and hemocytes. Dead cells were excluded from the flow cytometric analysis on the basis of propidium iodide staining (2 μg/ml). Flow cytometry was performed using a Cytomation MoFlo and data were analyzed with Cytomation Summit software.

Detection of K-ras mutations. PCR-amplified DNA samples from spontaneous adenocarcinomas and the corresponding non-tumorous lung tissues from 6 *SOPten*$^{flox/flox}$(P21–P27) mice were analyzed to detect *K-ras* mutations as described previously (43). Briefly, direct sequence analysis was performed to examine the first exon (spans the region containing codons 12 and 13) and second exon (spans the region containing codon 61) of the *K-ras* oncogene. The primers used to amplify the DNAs of first and second *K-ras* exons as well as the primers for these DNAs sequences are listed in Supplemental Table 1.

Statistics. Statistical differences were determined using the 2-tailed Student's t test or Welch's t test. A P value of less than 0.05 was considered statistically significant.

Acknowledgments

We thank Tetsuo Noda (of the Cancer Institute of the Japanese Foundation for Cancer Research), Tomoharu Kanie, Nobuhiro Ban, Tae Inoue, Satoru Kawarasaki, Ryota Iizuka, Shinsuke Chida, Hiromi Takahashi, and Miyuki Natsui (all of Akita University) for helpful discussions and technical support. This work was supported by grants from the Ministry of Education, Science, Sports and Culture, Japan; the Novartis Foundation; the Yasuda Medical Foundation; and the Suzuken Memorial Foundation.

Received for publication February 16, 2007, and accepted in revised form July 12, 2007.

Address correspondence to: Akira Suzuki, Division of Embryonic and Genetic Engineering, Medical Institute of Bioregulation, Kyushu University, Maidashi 3-1-1, Higashi-ku, Fukuoka, Fukuoka 812-8582, Japan. Phone: 81-92-642-6838; Fax: 81-92-632-1499; E-mail: suzuki@bioreg.kyushu-u.ac.jp.

Shigehisa Yanagi and Hiroyuki Kishimoto contributed equally to this work as first authors.

Masamitsu Nakazato and Akira Suzuki contributed equally to this work as senior authors.

1. Jemal, A., Thomas, A., Murray, T., and Thun, M. 2002. Cancer statistics, 2002. *CA Cancer J. Clin.* **52**:23–47.
2. Giangreco, A., Groot, K.R., and Janes, S.M. 2007. Lung cancer and lung stem cells: strange bedfellows? *Am. J. Respir. Crit. Care Med.* **175**:547–553.
3. Minna, J.D., Roth, J.A., and Gazdar, A.F. 2002. Focus on lung cancer. *Cancer Cell.* **1**:49–52.
4. Reya, T., Morrison, S.J., Clarke, M.F., and Weissman, I.L. 2001. Stem cells, cancer, and cancer stem cells. *Nature.* **414**:105–111.
5. Kim, C.F., et al. 2005. Identification of bronchioalveolar stem cells in normal lung and lung cancer. *Cell.* **121**:823–835.
6. Maehama, T., and Dixon, J.E. 1998. The tumor suppressor, PTEN/MMAC1, dephosphorylates the lipid second messenger, phosphatidylinositol 3,4,5-trisphosphate. *J. Biol. Chem.* **273**:13375–13378.
7. Cantley, L.C. 2002. The phosphoinositide 3-kinase pathway. *Science.* **296**:1655–1657.
8. Gerber, H.P., et al. 1998. Vascular endothelial growth factor regulates endothelial cell survival through the phosphatidylinositol 3′-kinase/Akt signal transduction pathway. Requirement for Flk-1/KDR activation. *J. Biol. Chem.* **273**:30336–30343.
9. Groszer, M., et al. 2006. PTEN negatively regulates neural stem cell self-renewal by modulating G0-G1 cell cycle entry. *Proc. Natl. Acad. Sci. U. S. A.* **103**:111–116.
10. Wang, S., et al. 2006. Pten deletion leads to the expansion of a prostatic stem/progenitor cell subpopulation and tumor initiation. *Proc. Natl. Acad. Sci. U. S. A.* **103**:1480–1485.
11. Yilmaz, O.H., et al. 2006. Pten dependence distinguishes haematopoietic stem cells from leukaemia-initiating cells. *Nature.* **441**:475–482.
12. Kimura, T., et al. 2003. Conditional loss of PTEN leads to testicular teratoma and enhances embryonic germ cell production. *Development.* **130**:1691–1700.
13. Forgacs, E., et al. 1998. Mutation analysis of the PTEN/MMAC1 gene in lung cancer. *Oncogene.* **17**:1557–1565.
14. Marsit, C.J., et al. 2005. PTEN expression in non-small-cell lung cancer: evaluating its relation to tumor characteristics, allelic loss, and epigenetic alteration. *Hum. Pathol.* **36**:768–776.
15. Tang, J.M., He, Q.Y., Guo, R.X., and Chang, X.J. 2006. Phosphorylated Akt overexpression and loss of PTEN expression in non-small cell lung cancer confers poor prognosis. *Lung Cancer.* **51**:181–191.
16. Han, S., Khuri, F.R., and Roman, J. 2006. Fibronectin stimulates non-small cell lung carcinoma cell growth through activation of Akt/mammalian target of rapamycin/S6 kinase and inactivation of LKB1/AMP-activated protein kinase signal pathways. *Cancer Res.* **66**:315–323.
17. Hagenbeek, T.J., et al. 2004. The loss of PTEN allows TCR alphabeta lineage thymocytes to bypass IL-7 and Pre-TCR-mediated signaling. *J. Exp. Med.* **200**:883–894.
18. Suzuki, A., et al. 2003. Critical roles of Pten in B cell homeostasis and immunoglobulin class switch recombination. *J. Exp. Med.* **197**:657–667.
19. Hamada, K., et al. 2005. The PTEN/PI3K pathway governs normal vascular development and tumor angiogenesis. *Genes Dev.* **19**:2054–2065.
20. Warburton, D., et al. 2000. The molecular basis of lung morphogenesis. *Mech. Dev.* **92**:55–81.
21. Luukko, K., Ylikorkala, A., Tiainen, M., and Makela, T.P. 1999. Expression of LKB1 and PTEN tumor suppressor genes during mouse embryonic development. *Mech. Dev.* **83**:187–190.
22. Sauer, B. 1998. Inducible gene targeting in mice using the Cre/lox system. *Methods.* **14**:381–392.
23. Perl, A.K., Wert, S.E., Nagy, A., Lobe, C.G., and Whitsett, J.A. 2002. Early restriction of peripheral and proximal cell lineages during formation of the lung. *Proc. Natl. Acad. Sci. U. S. A.* **99**:10482–10487.
24. Suzuki, A., et al. 2001. T cell-specific loss of Pten leads to defects in central and peripheral tolerance. *Immunity.* **14**:523–534.
25. Yamada, M., Kurihara, H., Kinoshita, K., and Sakai, T. 2005. Temporal expression of alpha-smooth muscle actin and drebrin in septal interstitial cells during alveolar maturation. *J. Histochem. Cytochem.* **53**:735–744.
26. Compernolle, V., et al. 2002. Loss of HIF-2alpha and inhibition of VEGF impair fetal lung maturation, whereas treatment with VEGF prevents fatal respiratory distress in premature mice. *Nat. Med.*

8:702–710.
27. Tefft, J.D., et al. 1999. Conserved function of mSpry-2, a murine homolog of Drosophila sprouty, which negatively modulates respiratory organogenesis. *Curr. Biol.* **9**:219–222.
28. Mailleux, A.A., et al. 2001. Evidence that SPROUTY2 functions as an inhibitor of mouse embryonic lung growth and morphogenesis. *Mech. Dev.* **102**:81–94.
29. Bellusci, S., et al. 1997. Involvement of Sonic hedgehog (Shh) in mouse embryonic lung growth and morphogenesis. *Development.* **124**:53–63.
30. Litingtung, Y., Lei, L., Westphal, H., and Chiang, C. 1998. Sonic hedgehog is essential to foregut development. *Nat. Genet.* **20**:58–61.
31. Malkinson, A.M., and Beer, D.S. 1983. Major effect on susceptibility to urethan-induced pulmonary adenoma by a single gene in BALB/cBy mice. *J. Natl. Cancer Inst.* **70**:931–936.
32. Goodell, M.A., Brose, K., Paradis, G., Conner, A.S., and Mulligan, R.C. 1996. Isolation and functional properties of murine hematopoietic stem cells that are replicating in vivo. *J. Exp. Med.* **183**:1797–1806.
33. Reynolds, S.D., et al. 2007. Molecular and functional properties of lung SP cells. *Am. J. Physiol. Lung Cell. Mol. Physiol.* **292**:L972–L983.
34. Summer, R., Kotton, D.N., Sun, X., Ma, B., Fitzsimmons, K., and Fine, A. 2003. Side population cells and Bcrp1 expression in lung. *Am. J. Physiol. Lung Cell. Mol. Physiol.* **285**:L97–L104.
35. Paling, N.R., Wheadon, H., Bone, H.K., and Welham, M.J. 2004. Regulation of embryonic stem cell self-renewal by phosphoinositide 3-kinase-dependent signaling. *J. Biol. Chem.* **279**:48063–48070.
36. Satoh, Y., et al. 2004. Roles for c-Myc in self-renewal of hematopoietic stem cells. *J. Biol. Chem.* **279**:24986–24993.
37. Taipale, J., and Beachy, P.A. 2001. The Hedgehog and Wnt signalling pathways in cancer. *Nature.* **411**:349–354.
38. Domen, J., Gandy, K.L., and Weissman, I.L. 1998. Systemic overexpression of BCL-2 in the hematopoietic system protects transgenic mice from the consequences of lethal irradiation. *Blood.* **91**:2272–2282.
39. Walkley, C.R., Fero, M.L., Chien, W.M., Purton, L.E., and McArthur, G.A. 2005. Negative cell-cycle regulators cooperatively control self-renewal and differentiation of haematopoietic stem cells. *Nat. Cell Biol.* **7**:172–178.
40. Wu, W., Fan, Y.H., Kemp, B.L., Walsh, G., and Mao, L. 1998. Overexpression of cdc25A and cdc25B is frequent in primary non-small cell lung cancer but is not associated with overexpression of c-myc. *Cancer Res.* **58**:4082–4085.
41. Pezzella, F., et al. 1993. bcl-2 protein in non-small-cell lung carcinoma. *N. Engl. J. Med.* **329**:690–694.
42. Rodenhuis, S., et al. 1988. Incidence and possible clinical significance of K-ras oncogene activation in adenocarcinoma of the human lung. *Cancer Res.* **48**:5738–5741.
43. You, M., et al. 1992. Parental bias of Ki-ras oncogenes detected in lung tumors from mouse hybrids. *Proc. Natl. Acad. Sci. U. S. A.* **89**:5804–5808.
44. Wang, J., et al. 2005. PI3K-AKT pathway mediates growth and survival signals during development of fetal mouse lung. *Tissue Cell.* **37**:25–35.
45. Stambolic, V., et al. 1998. Negative regulation of PKB/Akt-dependent cell survival by the tumor suppressor PTEN. *Cell.* **95**:29–39.
46. Backman, S.A., et al. 2001. Deletion of Pten in mouse brain causes seizures, ataxia and defects in soma size resembling Lhermitte-Duclos disease. *Nat. Genet.* **29**:396–403.
47. Stepan, V., et al. 2005. Regulation and function of the sonic hedgehog signal transduction pathway in isolated gastric parietal cells. *J. Biol. Chem.* **280**:15700–15708.
48. Blenkinsopp, W.K. 1967. Proliferation of respiratory tract epithelium in the rat. *Exp. Cell Res.* **46**:144–154.
49. Jackson, E.L., et al. 2001. Analysis of lung tumor initiation and progression using conditional expression of oncogenic K-ras. *Genes Dev.* **15**:3243–3248.
50. Lapidot, T., et al. 1994. A cell initiating human acute myeloid leukaemia after transplantation into SCID mice. *Nature.* **367**:645–648.
51. Al-Hajj, M., Wicha, M.S., Benito-Hernandez, A., Morrison, S.J., and Clarke, M.F. 2003. Prospective identification of tumorigenic breast cancer cells. *Proc. Natl. Acad. Sci. U. S. A.* **100**:3983–3988.
52. Singh, S.K., et al. 2004. Identification of human brain tumour initiating cells. *Nature.* **432**:396–401.
53. Kohno, T., Takahashi, M., Manda, R., and Yokota, J. 1998. Inactivation of the PTEN/MMAC1/TEP1 gene in human lung cancers. *Genes Chromosomes Cancer.* **22**:152–156.
54. Sibilia, M., et al. 2000. The EGF receptor provides an essential survival signal for SOS-dependent skin tumor development. *Cell.* **102**:211–220.
55. Gille, H., and Downward, J. 1999. Multiple ras effector pathways contribute to G(1) cell cycle progression. *J. Biol. Chem.* **274**:22033–22040.
56. Gregory, M.A., Qi, Y., and Hann, S.R. 2003. Phosphorylation by glycogen synthase kinase-3 controls c-myc proteolysis and subnuclear localization. *J. Biol. Chem.* **278**:51606–51612.
57. Barata, J.T., et al. 2004. Activation of PI3K is indispensable for interleukin 7-mediated viability, proliferation, glucose use, and growth of T cell acute lymphoblastic leukemia cells. *J. Exp. Med.* **200**:659–669.
58. Wert, S.E., Glasser, S.W., Korfhagen, T.R., and Whitsett, J.A. 1993. Transcriptional elements from the human SP-C gene direct expression in the primordial respiratory epithelium of transgenic mice. *Dev. Biol.* **156**:426–443.
59. Suzuki, A., et al. 1998. High cancer susceptibility and embryonic lethality associated with mutation of the PTEN tumor suppressor gene in mice. *Curr. Biol.* **8**:1169–1178.
60. Horie, Y., et al. 2004. Hepatocyte-specific Pten deficiency results in steatohepatitis and hepatocellular carcinomas. *J. Clin. Invest.* **113**:1774–1783. doi:10.1172/JCI200420513.